Arch Appl Mech (2021) 91:2039–2052
https://doi.org/10.1007/s00419-020-01868-z

ORIGINAL

Prafulla Kumar Swain · **Siva Prasad Dora**

Experimental and numerical investigation of wing–wing interaction and its effect on aerodynamic force of a robotic dragonfly during hovering and forward flight

Received: 14 August 2020 / Accepted: 12 December 2020 / Published online: 7 January 2021

Abstract In the present study, a flapping-wing micro-air vehicle (FWMAV) like a dragonfly is developed by changing the phase shift angle between the fore and hind wings and experimentally tested using the wind tunnel. Two conditions are considered while conducting the experiments; (1) hovering [advance ratio (J) or the inlet velocity of air is kept zero], and (2) forward flight condition (advance ratio $J = 0.4$). Four phase angles (γ) are considered in the experiment analysis (0°, 60°, 90°, and 180°). For the validation of experimental results, computational fluid dynamics (CFD) analysis was executed by implementing fluid–structure interaction method. It is observed that the in-phase flapping ($\gamma = 0°$) generates larger force and at the same time produces larger variation of force over the entire flapping cycle. This condition is suitable for take-off and forward flight of the dragonfly. In the counter-phase/out of phase ($\gamma = 180°$), the magnitude of force generated is less as compared to the in-phase flapping. However, the counter-phase condition is more stable as compared to in phase flapping, and thus, it is more suitable for hovering flight of the dragonfly. The time of interaction of wake capture, wing–wing interaction, and dipole structure are examined through 2-D vorticity flow fields around the fore and hind wings. The obtained CFD results are in close agreement with the experimental results.

Keywords Forewing · Hindwing · Phase angle · Flapping wing · FWMAV · In-phase · Counter-phase · Vorticity

1 Introduction

Dragonflies are extremely capable flyers exhibiting a range of flight manoeuvers. Gliding, hovering, forward flight, sharp turning, accelerated flight, and backward flight are examples of such manoeuvers, which are well studied by different researchers across the globe [1–5]. The complex flight manoeuvers of dragonfly distinguish it from other insect like butterflies and bees, etc. [2–6]. It can independently control the individual wing movement. One of the key features, which play a significant role in different flight mode of a dragonfly, is the phase modulation between the forewing and hindwing. The in-phase, out-of-phase and hindwing leading the forewing are important phase modulation, which the dragonflies use frequently during the different flight modes. From the previous research study [7–10], it is revealed that the in-phase flapping is beneficial for high lift and thrust, whereas counter-phase flapping is more suitable for stable flight like hovering. It is reported by few researchers [11–16] the wing–wing synergy with phase modulation between wings is beneficial for hovering flight.

The experimental analysis and two-dimensional simulation method by Wang and Russell [17] for a hovering dragonfly revealed that the counter-phase flapping is suitable for less power consumption with a stable floating of wings. Similar experiment was also conducted by Usherwood and Lehmann [18]. Their results showed

P. K. Swain (✉) · S. P. Dora
Department of Mechanical Engineering, GIT, GITAM (Deemed To Be University), Visakhapatnam, Andhra Pradesh, India
e-mail: kprafull@gitam.edu

that during hindwing lead forewing condition the power consumption is reduced by 19% as compared to the forewing lead the hindwing. The 2-D simulation performed by Lua et al. [19] of a tandem flapping wing in forward flight revealed that the thrust elicited can be either reduce or enhance compared to the single wing thrust depending on the interact of forewing wake to the hindwing.

A dragonfly can change the circulation generated around the wings by adjusting the pitch angle with their flexible wings [10, 19]. When the dragonfly flaps its wing at higher angle of attack, the flow around wing tip separates and reattaches to form a vortex called leading edge vortex (LEV) [20]. The existence of LEV enhances the lift force of hindwing [21]. The LEV developed along the wing-span of a wing is well studied by Hefler et al. [22]. Their results showed that the LEV cannot develop at root of the wing. Furthermore, in the middle of the wing the forewing and hindwing interaction can reduce or enhance the hindwing LEV. But at outer region of the wing, there is a significant lift enhancement because of wake capture by hindwing shed by forewing. Forewing–hindwing synergy and vorticity flow fields are well studied by Hsieh et al. [23]. They found an interesting result at 90° and 180° phase modulation between forewing and hindwing. When both wings maintained at 90° phase between them and the shed trailing edge vortex is generated during downstroke of forewing interaction with the LEV of hind wing's upstroke, then there exits enhancement in thrust of the hindwings. However, when both the wings maintained an angle of 180° phase and shed trailing edge vortex of forewing during its downstroke merges with shed trailing edge vortex of hindwing, there occurs the lift enhancement. Even though there are varied views on how the presence and addition of the LEV contribute to force generation in insect wings such as lack of stall [24], enhancement of wing circulation, and suction [25], it is well identified by many researches [25–30] that the presence of LEV imparts larger momentum to the surrounding fluid leading to the generation of larger forces as compared to under steady-state conditions.

During flapping, the aerodynamic force in upstroke and downstroke varies rapidly because of the different wing kinematics, such as wingtip velocity and angle of attack. [30]. Most of the insects like dragonflies, damselflies, etc., produce larger lift force in downstroke as compared to upstroke during hovering and foreword flight, as the wing-tip velocity and angle of attack are usually more in downstroke as compared to upstroke. Hence, the wing tip covers a shorter trajectory during upstroke because of smaller angle of attack and wing-tip velocity [31]. Bomphrey et al. [32] studied the forward flight of a dragonfly. Their result showed that the leading edge vortex generated during the forward flight at forewing was sufficient alone to hold the weight of the dragonfly. They also reported that tandem wings were less efficient than single wing in forward flight. The effect of phase modulation on lift in forward flight of a dragonfly is studied by Broering et al. [33], and they revealed that the hindwing lift is enhanced at in-phase where there is decrease in lift at counter-phase and 90° phase angle. The 2-D, PIV experiment study conducted by Rival et al. [34–36] concluded that lift and thrust of hindwing depend on the upwash and downwash flow of the trialing edge vortex (TEV) generated by forewing.

Most of the studies were concern on either purely experimental or numerical investigation. But none of the studies were carried out on the investigation of robotic dragonfly model using both experimental and numerical analysis simultaneously. In the present study, both experiment and numerical investigations are performed with different phase modulation between the forewing and hindwings in hovering as well as forward flight. It is found from the present investigation that the in-phase flapping results in high lift and drag with a instability during the flapping, whereas the out of phase results in a low lift with almost zero drag, but maintains stability throughout the flapping cycle. Both experiment and numerical simulation results are in close agreement with each other.

2 Material and methods

2.1 Details of micro-aerial vehicle

The details of the present FWMAV like dragonfly are compared with other similar kind of FWMAV developed by different authors in various features, such us wing span, flapping frequency, Reynolds Number (Re), reduced number (k), etc., as shown in Table 1. The design concept of flapping mechanism of dragonfly is influenced by insect flapping wing flight. The FWMAV developed for experiment is shown in Fig. 1a, b which consists of flapping mechanism, power module and wing design.

2.1.1 Flapping mechanism

A 4-bar slider crank mechanism is designed to provide the flapping motion to the wings of the dragonfly model. It consists of a connecting rod, crank, gear mechanism and leading edge of the wings as shown in Fig. 1a, b.

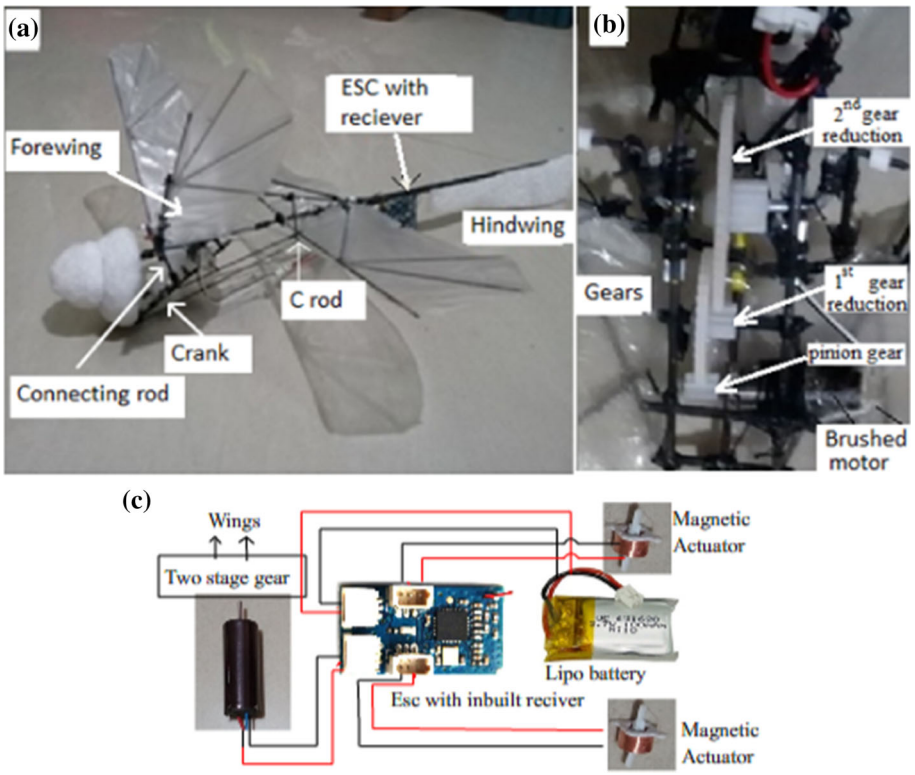

Fig. 1 Dragonfly MAV **a** a closer view, **b** micro-gear box made with rod, **c** electronic circuit of power module

Table 1 Characteristics of two dragonfly species [10, 11], experimental model [37] and present dragonfly prototype

Characteristics dragonfly species	Unit	Azuma et al. (1985)	Azuma and Watanabe	Takahashi et al	Present FWMAV
Wing span	mm	66	107	276	250
Aspect ratio		9	8.9	6.9	8.1
Frequency	Hz	41.5	27.7	12	12
Amplitude	Degree	5	29.5	30	55
Wing load	N/mm^2	2.6	3.5	4.6	5.2
Re		1737	1721	1670	2365
k		0.14	0.19	0.28	0.128

A micro-gear casing is developed using thin carbon rod-tube with thread and CI glue. Usually, the adhesive is used in fabrication of FWMAV to minimize the weight of the gear box. Nylon gears are used to transmit the rotational power of the motor to wings through the 4-bar slider crank mechanism with a gear ratio of 1:28. The number of teeth on motor pinion, first gear, intermediate pinion and second gears is 8, 40, 10, 56 respectively. A closer view of the micro-gear cashing is shown in Fig. 1b. The power module consists of Lipo battery, brushed motor, micro-electronic speed controller (ESC) with receiver, magnetic actuator and transmitter. The details of the electronic components and the power circuit are shown in Fig. 1c. Brushed motor (8 mm diameter having 4 gm) draws power from Lipo battery (3.7 V, 100 mah, 3.2 gm) through 1 gm electronic speed controller (ESC), which is controlled by the transmitter. For steering of the FWMAV two micro-magnetic actuators weighting only 0.36 gm are used at the hindwing.

2.1.2 Wing design

Figure 2a, b shows the schematic diagram of a dragonfly with stroke plane. It also shows the positive phase shift angle (hindwing lead the forewing) and negative phase shift angle (forewing lead the hindwing). The wing is developed from carbon fiber rod as skeleton and thin Mylar sheet of thickness of 51 μm is used as the

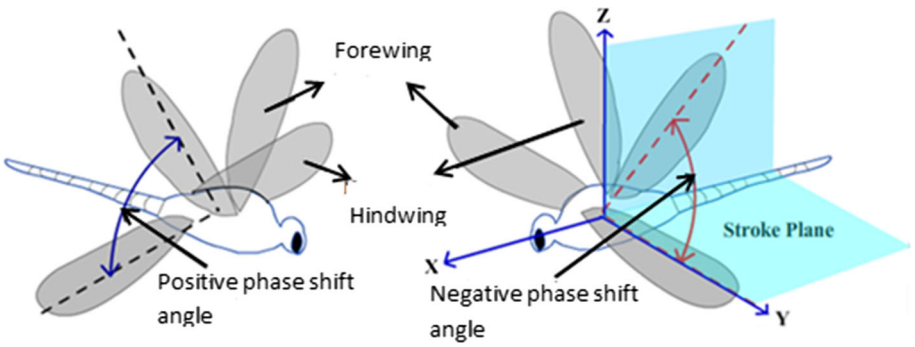

Fig. 2 Forewing and hindwing with phase angle

skin of wings. The leading edge support is made up of 1-mm-diameter carbon-fiber rod, whereas the diagonal support rib is made up of 0.5 mm carbon rod. To maintain a desired phase shift angle between the forewing and hindwing, a diagonal rod called 'C" rod is used which connects the two wings as shown in Fig. 1a. The wings can flap about a pivot point along the stroke plane. A carbon rod of 1.5 mm diameter is used to support the fuselage of the dragonfly. The wings are separated by a small distance of 1.4 cm (where c_m is the mean chord length) along the longitudinal axis. The wing span of forewing and hindwing is 210 mm and 250 mm, respectively. The chord length of forewing (c_f) and hindwing (c_h) is 40 mm and 45 mm, respectively; hence mean chord length (average of c_f and c_h) is taken as 42.5 mm. The total surface area of the wing is 1936 mm^2 and the total flying weight is 16.5 gm. The flapping angle for forewing is 35° to − 20° and for hindwing 10° to − 45°. The tested model has flapping frequency of 12 Hz with a maximum wing load of 5.2 N/m^2. The inlet velocity is the velocity of the air in the wind tunnel, and the surrounding fluid is air. The Reynolds number is defined as $Re = U_{tip}c_m/v$, where v is the kinematic viscosity (1.56×10^{-5} for air at room temperature). The average wing tip velocity (U_{tip}) of the forewing is measured as 0.868 ms^{-1}.

2.1.3 Experimental setup

The experiment is carried out inside a wind tunnel by keeping the model over a load cell. The experiment is repeated by changing the forewing and hindwing position so as to get the required phase angle between them. The inlet velocity of the air is varied during forward flight condition from 2 to 8 m/s, whereas for hovering flight the inlet velocity is kept zero. A six-axis force/torque sensor (ATI Nano-17) is used to measure the induced force along the vertical and horizontal directions. The resolution and the frequency of this sensor are 1/64 N-mm and 1 kHz, respectively. The force generated during flapping is captured using a PCI DAQ card, and then transferred to a desktop for data storage and further analysis as shown in Fig. 3. A high-speed camera (512 PCI) is used to record the wing position at frame rate of 2000 frames per second with 512×512 pixels resolution. The data obtained from PCI DAQ and camera image are then correlated according to the motion of the wing. The flapping frequency of the wing is controlled through a transmitter located outside. Two separate desktop computers have been used to capture the data from the camera as well as the load cell.

2.2 Simulation analysis by using fluid structure interaction (FSI)

Commercial solver ANSYS-FLUENT and ANSYS-TRNSIENT STRUCTURAL are used to simulate the model in a fluid domain. A 3-D model as shown in Fig. 4 is developed in a CATIA, and transferred to fluent geometry module, which is shared between transient structural solver and fluent solver. The computational domain is a cubic of side 50 cm. The inlet velocity of air is varied from zero (hovering) to 8 m/s (forward flight condition). Free-slip wall conditions are selected to all other sides, and a zero-gauge-pressure condition at outer boundary. The fluid domain is meshed with unstructured tetrahedral cells as these elements are good for complex geometry and dynamic grid [38]. Near the wing the mesh is refined so as to get a better convergence in the solution process. Transient solution with first order, Spalart–Allmaras model is considered in fluent setup as this model is suitable for unsteady flow structures [39]. The incompressible 3D Navier–Stokes equations and the equation of continuity presented in Eqs. 1 and 2 are solved by three-dimensional finite volume method.

$$\nabla . u = 0 \tag{1}$$

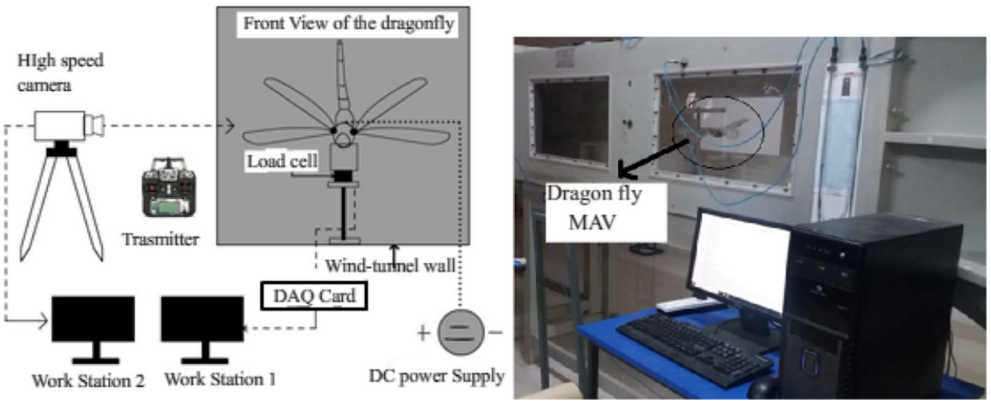

Fig. 3 Schematic view of the experimental setup

Table 2 Parameters of estimated functions for flapping, sweeping, rotation motion

Parameter	Representation	Forewing	Hind wing
Mid-stroke flapping amplitude	θ_{mf}	− 25.0	− 15.0
Flapping amplitude at time t	θ_{f}	28.0	34.0
Mid-stroke sweeping amplitude	θ_{ms}	1.5	-3
Sweeping amplitude at time *t*	θs	2	5
Mid-stroke rotational amplitude	θ_{mr}	52	26
Rotational amplitude at time *t*	θr	97	90
Adjustment sweeping parameter	*S*	0.25	0.32
Adjustment rotational parameter	*B*	2.2	2.6
Adjustment rotational parameter	*C*	2.5	3.2
Adjustment rotational parameter	*D*	4.6	5.2

$$\rho\frac{\mathrm{D}u}{Dt}+\rho\,\dot{\Omega}\times r+\rho\Omega\times(\Omega\times r)+2\rho\Omega\times u=-\nabla p+\mu\nabla^2 u \tag{2}$$

where ρ denotes the air density, u local velocity, t time, Ω angular velocity, $\dot{\Omega}$ angular acceleration, r position vector, p pressure, μ the dynamic viscosity of the air, and ∇ and ∇^2 gradient operator and Laplace operator, respectively. During pressure–velocity coupling, the least square method is used for gird solving. Second-order upwind sachems are selected to solve pressure and momentum equations. Figure 4c, d shows the wing tip trajectory and various wing kinematics of 3-D flapping wing. Three angles of wing motions relative to the stroke plane are: (1) flapping angle (ϕ), (2) swapping angle (φ) and (3) rotation angle (ψ). The colored dashed lines illustrate the forward stroke (blue colored), the supination (green colored), backward stroke (red colored) and pronation (purple colored), and the configuration of wing tip motion looks like a digit "8". Figure 4d represents the plane of flapping stroke. The equations of motions at boundary wing are given as follows.

$$\text{Flapping angle, } \phi(\dot{t}) = \theta_{\mathrm{fm}} - \theta_{\mathrm{f}}\sin(2\pi f t) \tag{3}$$

$$\text{Deviation angle, } \varphi(t) = \theta_{\mathrm{sm}} - \theta_{\mathrm{s}}\sin(4\pi f t + S) \tag{4}$$

$$\text{Rotation angle, } \psi(t) = \theta_{\mathrm{rm}} + \frac{\theta_{\mathrm{r}}}{1+\left[\frac{f_c - C}{B}\right]^{2D}} - \omega_y \tag{5}$$

The boundary values of the various parameters used in the present numerical studies are presented in Table 2. A UDF (user defined function) is used to define the above three equations via a command DEFINE_CG_MOTION and complied in dynamic mesh settings. Transient structural solver is used for structural analysis as the wing is flexible. In this analysis, the mesh is modeled with six node linear triangular prism mesh element having approximately 1365 C3D6 (six-node linear triangular prism) elements.

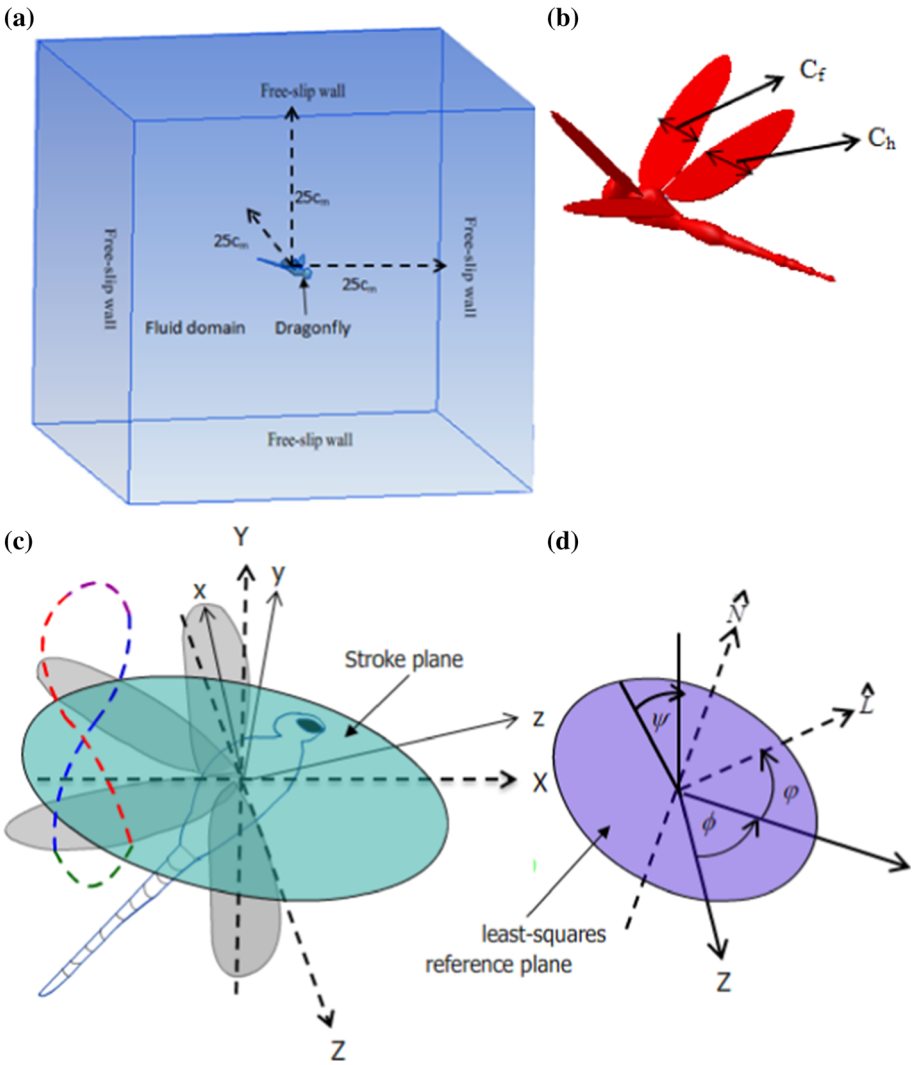

Fig. 4 **a** The dragonfly wing location and boundary condition in fluent environment, **b** enlarge view of the dragonfly developed in CATIA. **c** 3-D Flapping wing kinematics and three angle of wing motion relative to the stroke plane; flapping angle (ϕ), the swapping angle (φ) and the rotation angle (ψ). The colored dashed line illustrate the forward stroke (blue), the supination (green), backward stroke (red) and pronation (purple), **d** The least-square reference plane. (Color figure online)

2.2.1 Grid independence test

Figure 5a–c shows the grid independence test which is carried out with three different types of grid structure (coarse, medium and fine). The details of the number of cells used in the computational domain are presented in Table 3. A coarse grid is considered for initial solution. The number of cells in the computational domain is then gradually increased to increase the cell-density in the computational domain up to fine gird structure (9.1×10^6 cells) for further numerical investigation. Figure 5a–c shows the lift force in hovering and forward flight (for $J = 0.4$). From Fig. 5a it can be seen that, expect at $t/T = 0.4$ and 0.75 a negligible variation of lift is observed in hovering, however a consistent maximum lift was observed in forward flight as seen in Fig. 5b–c. The corresponding values are also tabulated in Table 3.

2.2.2 Validation of the experimental and numerical result

The present numerical simulation results are also validated with present experimental results. The total lift forces during hovering at the in-phase ($\gamma = 0°$) and thrust force in the forward flight ($J = 0.4$) obtained from experiments as well as from the numerical simulations are plotted in Fig. 6a–b. It can be seen from the graphs

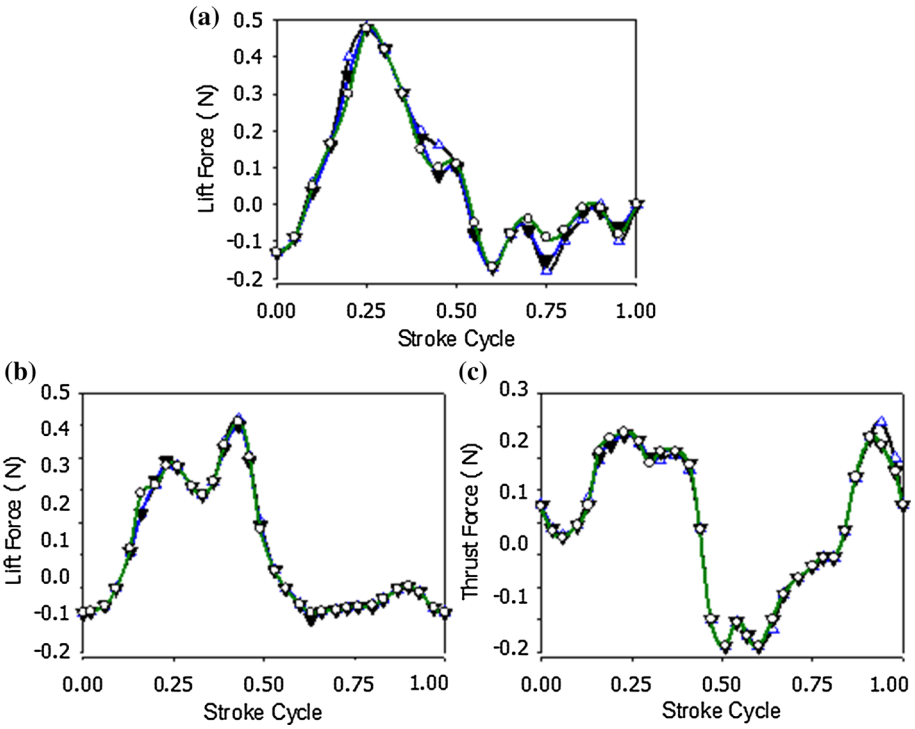

Fig. 5 Grid independence study: solid blue line, solid green line and solid black line represents the total lift for coarse, medium and fine grids, when the wing flaps at **a** total lift force during hovering, **b** lift force in forward flight, **c** thrust force in forward flight. (Color figure online)

Table 3 Forces obtained from three different grids

	No of grids cells	Maximum lift force (N) in hovering flight	Maximum lift force (N) in forward flight	Maximum thrust force (N) in forward flight
Coarse	2.1×106	0.478	0.423	0.213
Medium	5.3×10^6	0.486	0.453	0.243
Fine	9.1×10^6	0.488	0.457	0.213

that both experiment and numerical results are in close agreement with each other. Thus, the same numerical methodologies are used in our further analysis.

3 Results and discussions

During the experiment and simulation process, the hindwing leads the forewing condition is considered since this condition generates higher lift as compared to forewing leading the hindwing condition [13, 15, 37]. Further, the measurement of force is carried out for three conditions—(1) solo hindwing flapping; (2) solo forewing flapping; and (3) the combined action of the forewing and hindwing flapping. Different phase angles of 0°, 60°. 90° and 180° are kept between forewing and hindwing for our experiment as well as in numerical analyses.

3.1 Time-dependent aerodynamic force during the in-phase flapping

In the hovering condition, the inlet velocity in wind tunnel experiment as well as in fluent simulation is kept zero. Figure 7a–d shows the experimentally measured lift forces generated by the forewing and hindwing during hovering at different phase angles. Figure 7a shows the variation of lift force with the phase angle (γ) between the forewing and hind wing, when both the wings are flapping together. It can be seen form Fig. 7a

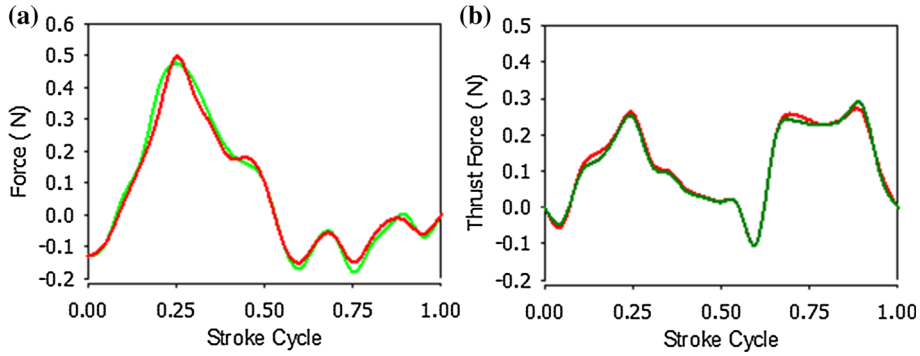

Fig. 6 Validation of experimental results with numerical simulation, red solid line represents experiment and green solid line represents simulation **a** total lift force in hovering, **b** thrust force in forward flight. (Color figure online)

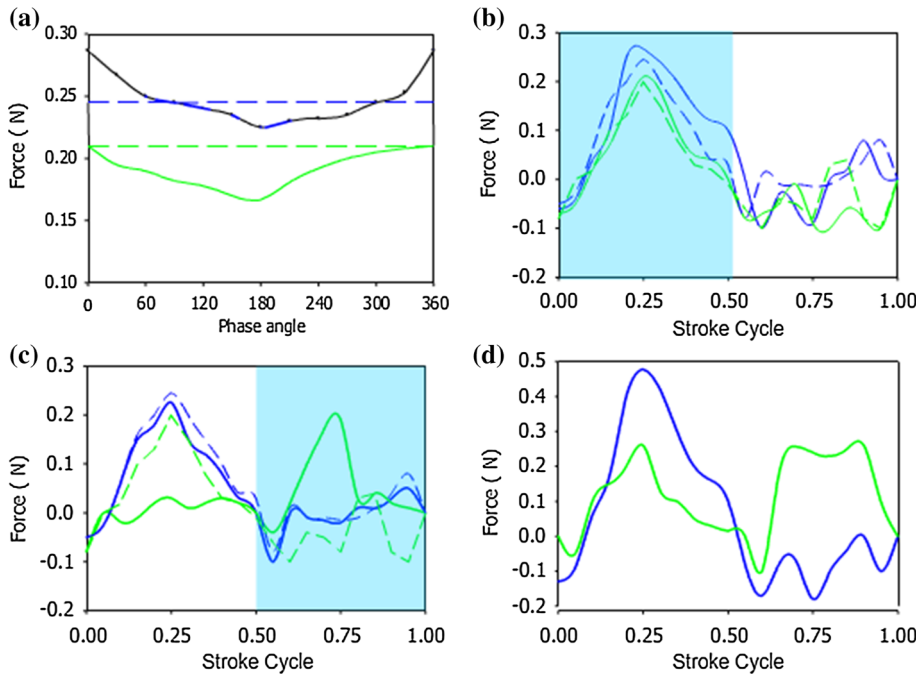

Fig. 7 Hovering flight experimental result with different phase modulation: Solid blue line and solid green line represent lift force of hindwing and forewing, respectively, when they flap together. Blue medium-dashed line and green medium-dashed line represent lift of hindwing and forewing, respectively, when flapping alone,. Shaded areas represent the downstroke of forewing. **a** Lift force of hindwing and forewing with different phase modulation when both wings flap together, **b** Hindwing lift at 0° phase with non-dimensional time, **c** Hindwing lift at 180° phase with non-dimensional time, **d** total lift of hindwing and forewing. (Color figure online)

that a high lift force is observed during the in-phase ($\gamma = 0°$ and 360°) flapping. However, the lift force is reduced at all other phase angles and a minimum value is reported at counter-phase ($\gamma = 180°$). To find out the effect of wing–wing interaction on aerodynamic forces, solo hindwing and solo forewing are flapped. Then the forces generated by the solo flapping conditions of the wing are subtracted from the wing–wing interaction condition so as to know how much force generated during the wing–wing interaction. It is observed that the lift force of solo wing condition is more than that of the wing–wing interaction condition at all phase angles expect (0° and 360°).

Figure 7b–d shows the variation of lift force of forewing, hindwing and total (sum of forewing and hindwing) at different time intervals of a single flapping cycle. When the wings are in-phase flapping, the lift force generated at hindwing and forewings is plotted in Fig. 7b. It can be seen that there exists a peak in lift force at $t/T = 0.25$. Since at this instant of time, the forewing and hindwing pass through the mid of down-stroke, which is responsible for creating the higher lift. (In Fig. 7 shaded area represents the downstroke of forewing).

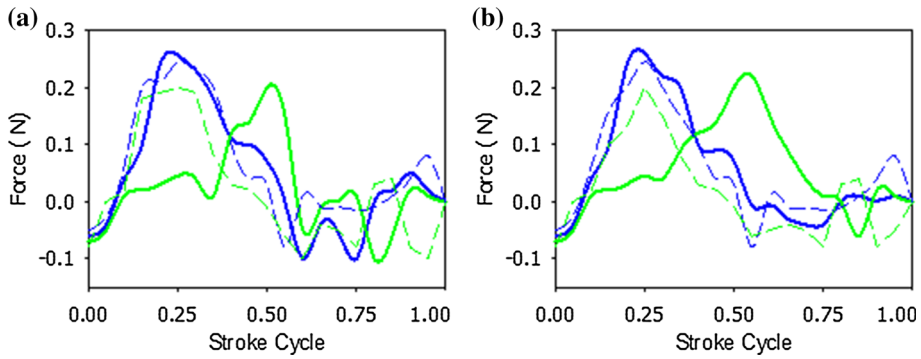

Fig. 8 Solid blue line and solid green line represent lift force of hindwing and forewing, respectively, when they flap together. Blue medium-dashed line and green medium-dashed line represent lift of hindwing and forewing, when they flap alone (No wing–wing interaction) respectively. **a** Lift of hindwing and forewing along time instant of stroke cycle while flapping together at phase angle of 60°, **b** lift of hindwing and forewing along time instant of stroke cycle while flapping together at phase angle of 90°. (Color figure online)

Two peaks in the lift force are observed in Fig. 7c when the wings are out of phase or counter-phase (flapping opposite to each other). These two peaks are due to hindwing downstroke (i.e. at $t/T = 0.25$) and downstroke of forewing ($t/T = 0.75$). Figure 7d shows the total lift force (sum of forewing and hind wing) with the stroke cycle. Similar trend is seen in the total lift force plot (one large lift for in-phase flapping and two average lift at counter-phase flapping).

It has been shown by the pervious researches [3, 18] that during hindwing leads the forewing flying condition, the phase angle in the range of 55°–100° is suitable for forward flight, whereas the phase angle of 180° is suitable for the hovering flight [6]. However, according to Ref. [19] the phase angle of 180° is also suitable for forward flight. Due to the conflicting results in phase angle by above researchers, we analyzed the effect of aerodynamic lift force at different phase angles of 60°, 90° along with the in-phase as well as the counter-phase. It is observed in Fig. 7c, d there are two peaks in lift for 180°, whereas there is a single large peak at 0° phase. When the phase angle is in between 0° and 180°, these peaks merge into a single large peak, which spreads wider in the entire stroke cycle as shown in Fig. 8a, b. When the phase angle is 60° (Fig. 8a), a single merged peak in lift is observed in between $t/T = 0$ and $t/T = 0.55$. For 90° phase angles, (Fig. 8b), the downstroke of hindwing is in between $t/T = 0$ and $t/T = 0.5$, but for forewing, it is in between $t/T = 0.25$ and $t/T = 0.75$, which results in the beginning of two peaks in between $t/T = 0$ and $t/T = 0.75$. In both the cases the lift generated due to wing–wing interaction is more as compared to single wing flapping (by observing blue medium-dashed line and green medium-dashed line that represents the lift of hindwing and forewing). Since in these entire phase angle the lift force generated by wings fluctuates along the stroke cycle, and hence 60° and 90° phase angles are not suitable for either hovering or forward flight condition.

3.2 Time-dependent aerodynamic force during the counter-phase flapping

In forward flight condition, the inlet velocities for both the wind tunnel experiment and the fluent simulations are varied so as to get the advance ratio of 0.4. The lift and thrust forces produced by forewing and hindwing during flapping at different phase angles in forward flight manoeuvers are shown in Fig. 9a–h. From Fig. 9a, b, it is observed that the lift of hindwing is reduced in forward flight as compared with hovering flight. But the magnitude of lift force is consistent with different phase modulations, which can be seen from Fig. 9 a, c, e, g. In case of forewing, the lift force is continuously varied with the phase angles. Similar to hovering condition, here also there exit two peaks in lift force at 180° (Fig. 9g) and one large peak at 0°(Fig. 9a) phase modulation. However, at 60° and 90° phase modulation the peak in the lift force (forewing) moves along the stroke cycle as shown in Fig. 9c, e respectively. The variation of peak is due to the variation in forewing lift force only.

Figure 9b, d, g, h represents the trust force generated in forewing and hindwing during different phase modulation. The thrust force of hindwing is varied by a significant amount from 0° to 180° phase, whereas a minor variation is observed for forewing at the same phase angles. From the experimental results, it is concluded that in-phase flapping of the dragonfly can generate a larger force as compared to the counter-phase flapping. But the in-phase flapping is more unstable (large variation in force) as compared to the counter-phase

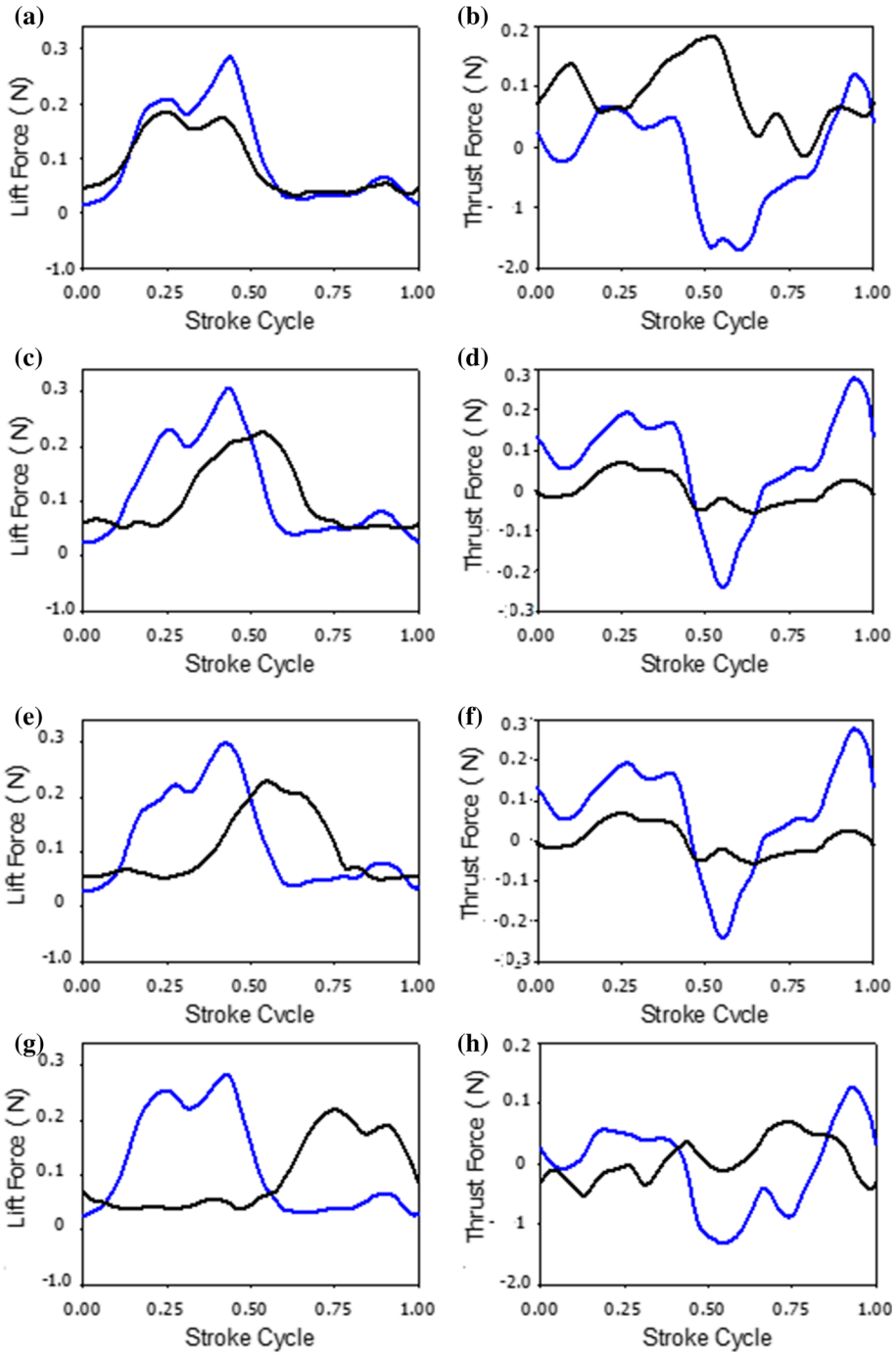

Fig. 9 Froward flight experiment result for advance ratio ($J = 0.4$) with stroke cycle (t/T): solid blue line and solid black represent force for hindwing and forewing, respectively, **a**–**h** represent the lift force and thrust force of hindwing and forewing at $\gamma = 0°$, 60°, 90°, and 180° respectively. (Color figure online)

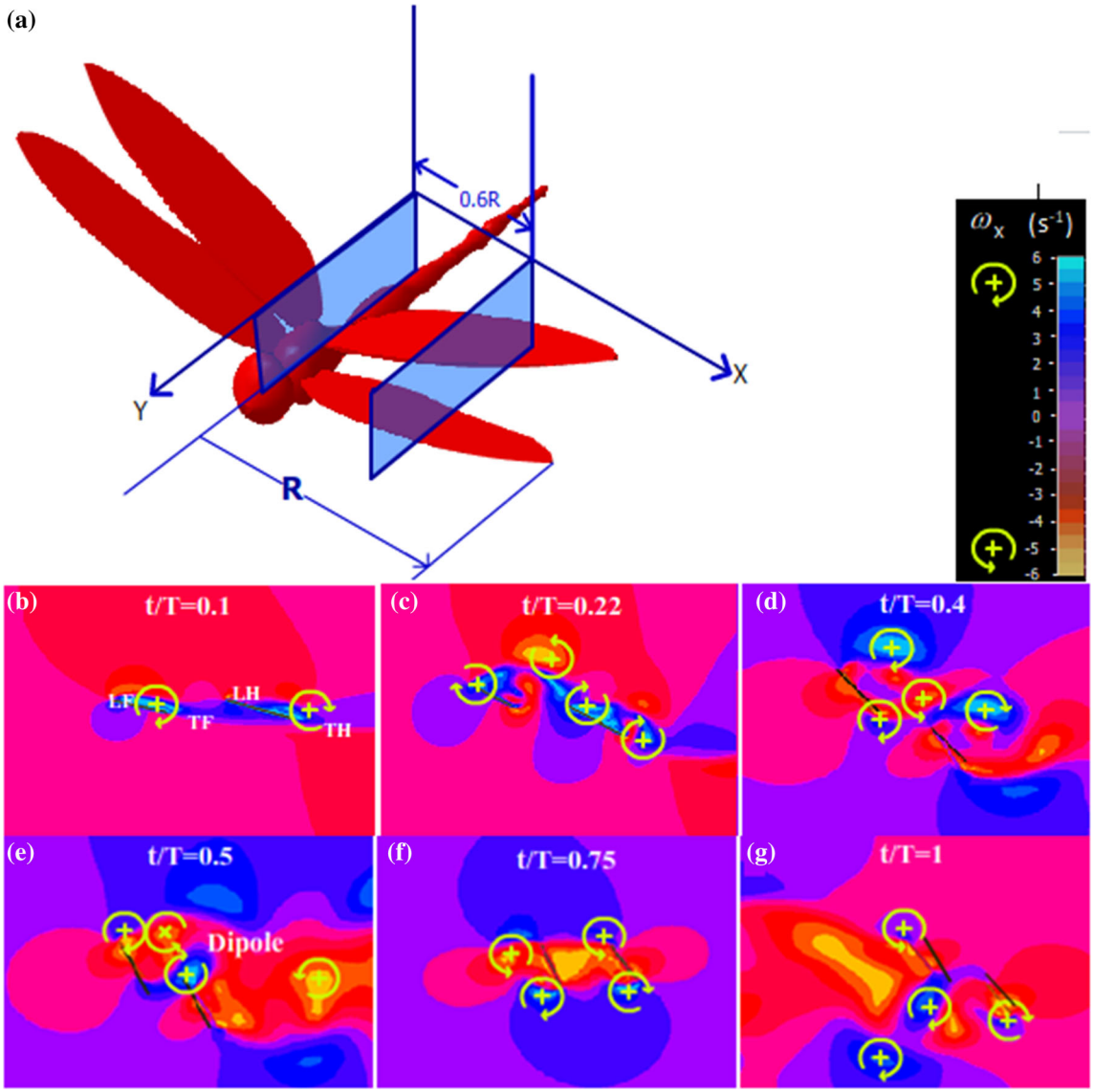

Fig. 10 Forward flight result corresponding to advance ratio $J = 0.4$. **a** Sectional view of the 3-D model, **b–g** time sequence of the wake produced by a forewing and hindwing during in-phase flapping in an air domain, the wing cross section is at a distance of $0.6R$ form wing root. The black lines vortex field represent chord of the wings, **b–d** complete half stroke (downstroke) of forewing–hindwing, **e** supination and **f–g** upstroke of the forewing–hindwing. In all the vorticity field + mark at blue indicate the origin of vortex and the direction arrow on the circle indicate direction of the spin of vortices. (Color figure online)

flapping. Hence, in-phase flapping is suitable for take-off and forward flights, which demand large forces. On the other hand the counter-phase flapping is suitable for hovering flight manoeuvers which demand a stable flight conditions.

3.3 Flow visualization through vortex structure in forward flight

To investigate the flow physics behind the lift enhancement of hindwing at in-phase flapping, during forward flight ($J = 0.4$), we captured vortex structures around the wings using the CFD simulation. Figure 10a shows the cross section of the wing at a distance of $0.6R$ (where 'R' is the distance of wing tip form the hinge point of flapping) from the root of the wing. Figure 10b–g shows the 2-D vorticity structures of the flow field at different time instants of a single flapping stroke around forewing and hindwing. LEVF/LEVH represent the

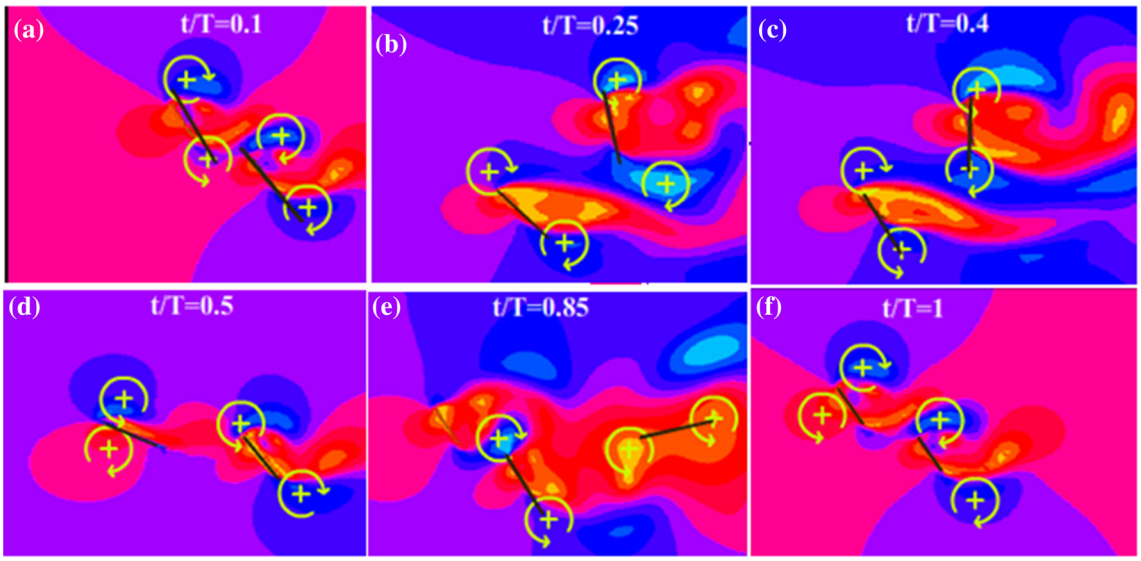

Fig. 11 Hovering flight result: time sequence of the wake produced by a forewing and hindwing during counter-phase flapping in an air domain, the wing cross section is at a distance of 0.6*R* form wing root. The black lines vortex field represent chord of the wings. **a**–**c** Complete half stroke (downstroke of hindwing and upstroke of forewing), **d** supination and **e**, **f** upstroke of the hind wing and downstroke of forewing. In all the vorticity field + mark at blue indicate the origin of vortex and the direction arrow on the circle indicate direction of the spin of vortices

leading edge vortex of forewing and TEVF/ TEVH represent the trailing edges vortex of forewing/hindwing. It is observed from Fig. 10b that two vortices are formed at the time cycle of $t/T = 0.5$—one clockwise vortex (CWV), and other one counter-clockwise vortex (CCWV) at the lead and trailing edge of both the wings. At the time instant $t/T = 0.4$, the forewing TEV (Trialing edge vortex) shades into the leading edge vortex (LEV) of hindwing. This shedding process is called the wake capture, which enhances the strength of the LEV of hind wing, which increases the total lift force. At $t/T = 0.5$ (the end of downstroke and beginning of upstroke) a further enhancement in lift force is observed since at this stage there occurs a sudden rotation of the wings due to supination. A similar observation was observed in our experimental results as shown in Fig. 9a, c, e, g. Because of sudden rotation of the wings, the vortex generated in both the wings is opposite in direction, resulting in the formation the dipole vortex structure as shown in Fig. 10e. During the time $t/T = 0.75$ both the wings are in mid of upstroke, and hence a less lift or wing–wing interaction is obtained as shown in Fig. 10e. At the end of upstroke or beginning of downstroke, there is a slight enhancement in lift force which is due to pronation effect as shown in Fig. 10g.

3.4 Discussion of lift force through vortex structure at counterstroke (hovering flight)

From the experimental results, it is concluded that the counter flapping is suitable for hovering flight as in this phase the lift force is more stable (less variation along the stroke cycle) compared to the in-phase flapping. Two important observations are reported from the experimental results; first, there is a reduction in hindwing lift force in the counter phase, and second, two peaks in the lift force in the flapping stroke. To understand the underline mechanisms, we extracted the vorticity field from CFD simulation, which is shown in Fig. 11a–f. At $t/T = 0.22$ the hindwing is at the mid-downstroke, resulting a high lift force for hindwing, but at same time instant, forewing is at mid of upstroke results in low lift force, as observed in Fig. 11b. At $t/T = 0.75$, the hindwing is at the mid-upstroke (low intensity of LEV can be seen near hindwing from Fig. 11c and at same instant the forewing is at mid of downstroke) (high intensity of LEV can be seen near forewing as shown in Fig. 11c). Hence, a minimum lift force is generated by hindwing and maximum lift force is generated by forewing. Therefore, two peaks in lift force are observed in counter flapping.

4 Conclusions

In the present study, the wing–wing interaction between forewing and hindwing of a robotic dragonfly is carried out by conducting experiment in wind tunnel. CFD simulation has also been carried out to validate the numerical results (vorticity flow study) with the experimental results by visualizing wing-induced vorticity field. The measurement of aerodynamic force is done for hovering and forward condition of the dragonfly model. It is concluded that, during in-phase flapping, the hind wing lift force is enhanced because of forewing LEV sheds into hindwing LEV. One large peak is observed at the in-phase flapping; whereas, two peaks in the lift force are observed at the counter phase flapping. Many mechanisms are revealed by inspecting the wake flow field around the forewing and hindwing, such as the dipole vortex formation and the wake capture. By observing the vorticity field at in-phase and counter-phase flapping, it is clear that the wings swept is limited in a small region at the in-phase flapping, whereas at counter-flapping it spread over larger area. Finally, it is clear from both the experiment and CFD results that in-phase flapping is suitable for forward flying and take-off conditions of a dragonfly because of higher lift generation. However, the counter-phase flapping generates a less lift force imparting more stability (less variation during the flapping stroke) for the hovering flying condition of the dragonfly.

Compliance with ethical standards

Conflict of interest All the authors declare that there is no conflict of interest.

References

1. Saharon, D., Luttges, M.W.: Dragonfly unsteady aerodynamics—the role of the wing phase relationship in controlling the produced flows. AIAA J. **89**, 1–19 (1989)
2. Alexander, D.E.: Unusual phase relationships between the forewings and hindwing in flying dragonflies. J. Exp. Biol. **109**, 379–383 (1984)
3. Thomas, A.L., Taylor, G.K., Srygley, R.B., Nudds, R.L., Bomphrey, R.J.: Dragonfly flight: free-flight and tethered flow visualizations reveal a diverse array of unsteady lift-generating mechanisms, controlled primarily via angle of attack. J. Exp. Biol. **207**, 4299–4323 (2004)
4. Fry, S.N., Sayaman, R., Dickinson, M.H.: The aerodynamics of free-flight maneuvers in Drosophila. Science **300**, 495–498 (2003)
5. Muijres, F.T., Elzinga, M.J., Melis, J.M., Dickinson, M.H.: Flies evade looming targets by executing rapid visually directed banked turns. Science **344**, 172–177 (2014)
6. Fry, S.N., Sayaman, R., Dickinson, M.H.: The aerodynamics of hovering flight in Drosophila. J. Exp. Biol. **208**, 2303–2318 (2005)
7. Sun, M., Lan, S.L.: A computational study of the aerodynamic forces and power requirements of dragonfly *Aeschna juncea* hovering. J. Exp. Biol. **207**, 1887–1901 (2004)
8. Lai, G.J., Shen, G.X.: Experimental investigation on the wing–wake interaction at the mid stroke in hovering flight of dragonfly. Sci. China Phys. Mech. Astron. **55**, 2167–2178 (2012)
9. Wang, H., Zeng, L.J., Liu, H., Yin, C.Y.: Measuring wing kinematics, flight trajectory and body attitude during forward flight and turning maneuvers in dragonflies. J. Exp. Biol. **206**, 745–757 (2003)
10. Azuma, A., Watanabe, T.: Flight performance of a dragonfly. J. Exp. Biol. **137**, 221–252 (1988)
11. Azuma, A., Azuma, S., Watanabe, I., Furuta, T.: Flight mechanics of a dragonfly. J. Exp. Biol. **116**, 79–107 (1985)
12. Maybury, W.L., Lehmann, F.O.: The fluid dynamics of flight control by kinematic phase lag variation between two robotic insect wings. J. Exp. Biol. **207**, 4707–4726 (2004)
13. VandenBerg, C., Ellington, C.P.: The three-dimensional leading-edge vortex of a hovering model hawkmoth. Philos. Trans. R. Soc. Lond. Ser. B Biol. Sci. **352**, 329–340 (1997)
14. Sun, M., Huang, H.: Dragonfly forewing hindwing interaction at various flight speeds and wing phasing. AIAA J. **45**, 508 (2007)
15. Hu, Z., Deng, X.Y.: Aerodynamic interaction between forewing and hindwing of a hovering dragonfly. Acta. Mech. Sin. **30**, 787–799 (2014)
16. Sun, X., Gong, X., Huang, D.: A review on studies of the aerodynamics of different types of maneuvers in dragonflies. Arch. Appl. Mech. **87**, 521 (2017)
17. Wang, Z.J., Russell, D.B.: Effect of forewing and hindwing interactions on aerodynamic forces and power in hovering dragonfly flight. Phys. Rev. Lett. **148101**, 1–4 (2007)
18. Usherwood, J.R., Lehmann, F.O.: Phasing of dragonfly wings can improve aerodynamic efficiency by removing swirl. J. R. Soc. Interface **5**, 1303 (2008)
19. Lua, K.B., Lu, H., Zhang, X.H., Lim, T.T., Yeo, K.S.: Aerodynamics of two-dimensional flapping wings in tandem configuration. Phys. Fluids **28**, 121901 (2016)

20. Shahzad, A., Tian, F.-B., Young, J., Lai, J.C.S.: Effects of wing shape, aspect ratio and deviation angle on aerodynamic performance of flapping wings in hovering. Phys. Fluids **28**, 111901 (2016)
21. Park, H., Choi, H.: Kinematic control of aerodynamic forces on an inclined flapping wing with asymmetric strokes. Bioinspiration Biomimetics **7**, 016008 (2012)
22. Hefler, C., Qiu, H., Shyy, W.: Aerodynamic characteristics along the wing span of a dragonfly *Pantala flavescens*. J. Exp. Biol. **221**, 1-14 (2018)
23. Hsieh, C.T., Kung, C.F., Chang, C.C., Chu, C.C.: Unsteady aerodynamics of dragonfly using a simple wing-wing model from the perspective of force decomposition. J. Fluid Mech. **663**, 233–252 (2010)
24. Nabawy, M.R.A., Crowther, W.J.: The role of the leading edge vortex in lift augmentation of steadily revolving wings: a change in perspective. J. R. Soc. Interface **14**, 1-9 (2017)
25. Shyy, W., Liu, H.: Flapping wings and aerodynamic lift: the role of leading-edge vortices. AIAA J. **45**, 2817–2819 (2017)
26. Muijres, F., Johansson, L., Barfield, R., Wolf, M., Spedding, G., Hedenstro, M.A.: Leading-edge vortex improves lift in slow-flying bats. Science **319**, 1250–1253 (2008)
27. Ristroph, L., Bergou, A.J., Guckenheimer, J., Wang, Z.J., Cohen, I.: Paddling mode of forward flight in insects. Phys. Rev. Lett. **106**, 178103 (2011)
28. Sane, S.P.: The aerodynamics of insect flight. J. Exp. Biol. **206**, 4191–4208 (2003)
29. Chin, D.D., Lentink, D.: Flapping wing aerodynamics: from insects to vertebrates. J. Exp. Biol. **219**, 920–932 (2016)
30. Tsai, B.J., Fu, Y.C.: Design and aerodynamic analysis of a flapping- wing micro aerial vehicle. Aerosp. Sci. Technol. **13**, 383–392 (2009)
31. Ellington, C.: The aerodynamics of hovering insect flight. III. Kinematics. Philos. Trans. R. Soc. Lond. B **305**, 41–78 (1984)
32. Bomphrey, R.J., Nakata, T., Henningsson, P., Lin, H.-T.: Flight of the dragonflies and damselflies. Philos. Trans. R. Soc. B **371**, 20150389 (2016)
33. Broering, T.M., Lian, Y.S., Henshaw, W.: Numerical investigation of energy extraction in a tandem flapping wing configuration. AIAA J. **50**(11), 2295–2307 (2012)
34. Rival, D., Manejev, R., Tropea, C.: Measurement of parallel blade–vortex interaction at low Reynolds numbers. Exp. Fluids **49**(1), 89–99 (2010)
35. Rival, D., Hass, G., Tropea, C.: Recovery of energy from leading- and trailing-edge vortices in tandem-airfoil configurations. J. Aircr. **48**(1), 203–211 (2011)
36. Rival, D., Schonweitz, D., Tropea, C.: Vortex interaction of tandem pitching and plunging plates: a two-dimensional model of hovering dragonfly-like flight. Bioinspir. Biomim. **6**(1), 016008 (2011)
37. Takahashi, H., Concorde, A., Paik, J., Shimoyama, I.: The effect of the phase angle between the forewing and hindwing on the aerodynamic performance of a dragonfly-type ornithopter. Aerospace **3**, 1–15 (2016)
38. Takahashi, S., Monjugawa, I., Nakahashi, K.: Unsteady flow computation around moving multiple bodies using overset unstructured grids. Trans. Jpn. Soc. Aeronaut. Space Sci. **51**, 78–85 (2008)
39. Jones, M., Yamaleev, N.K.: The effect of a gust on the flapping wing performance. In: 50th AIAA Aerospace Sciences Meeting including New Horizons Forum and Aerospace Exposition, (AIAA), Reston, pp. 1080–1088 (2012)